Proceedings of the IEEE Energy Conversion Congress and Exposition (ECCE USA 2013), Denver, Colorado, USA,
September 15-19, 2013

Comparative Evaluation of T-Type Topologies Comprising Standard and Reverse-Blocking IGBTs

H. Uemura,
F. Krismer,
J. W. Kolar

Comparative Evaluation of T-Type Topologies Comprising Standard and Reverse-Blocking IGBTs

Hirofumi Uemura, Florian Krismer, and Johann W. Kolar
Power Electronic Systems Laboratory
Swiss Institute of Technology,
Physikstrasse 3
8092 Zurich, Switzerland
Email: uemura@lem.ee.ethz.ch, www.pes.ee.ethz.ch

***Abstract*—For a Three-Level Three-phase T-type (3LTTC) rectifier and inverter of a high efficiency Uninterruptible Power Supply (UPS) with an output power of $20\,\mathrm{kVA}$, most suitable semiconductor components are selected. For this purpose, this paper details conduction and switching loss models of T-type rectifiers and inverters, compares the total semiconductor losses achieved for RB-IGBTs and for different types of conventional IGBTs, and evaluates the improvements achieved if the Si rectifier diodes are replaced by SiC Schottky Barrier Diodes (SiC SBDs). The switching loss model is parameterized with measured switching losses. According to the results of this comparison, the rectifier preferably employs RB-IGBTs to realize the bi-directional switch and SiC SBDs for the rectifier diodes; switching frequencies up to $32.5\,\mathrm{kHz}$ are feasible for total semiconductor losses of the rectifier of $250\,\mathrm{W}$. For the inverter, a realization of the bi-directional switch using an anti-series connection of conventional IGBT / SiC SBD modules is found to be most suitable and facilitates a switching frequency of $19.7\,\mathrm{kHz}$ for maximum allowed losses of $250\,\mathrm{W}$.**

I. Introduction

Uninterruptible Power Supply (UPS) systems ensure uninterruptible operation of highly available equipment, for example IT equipment of a data center, from a mains failure. For critical loads which need low input voltage distortion, a back-to-back configuration, as shown in Fig. 1, is often employed, since this configuration effectively suppresses mains voltage distortions; such UPS systems are called online or double conversion systems [1].

The investigated UPS system is an online UPS according to Fig. 1 with a rated power of $20\,\mathrm{kVA}$. The rms input and output line-to-neutral voltages of the considered system are $230\,\mathrm{V}$, the input and output frequencies are $50\,\mathrm{Hz}$, and the dc bus voltage is kept constant at $V_{\mathrm{dc}} = 720\,\mathrm{V}$. Rectifier and inverter stages of this UPS are designed for high efficiency, since, during normal mode of operation, both stages may be continuously operated up to nominal power.

Typical three-phase rectifier and inverter topologies include conventional two-level topologies and three-level neutral point clamped (NPC) topologies [2]. Three-phase two-level converters feature a low number of diodes (rectifier) or IGBTs (inverter) with maximum blocking voltages of $1200\,\mathrm{V}$ in the considered system and generate low conduction losses [3]. Two-level converters, however, require a comparably large EMI filter due to the high generation of harmonic content [4]. Three-level NPC inverters and rectifiers cause less harmonic content and, thus, allow for a reduced EMI filtering effort. These converters, however, require more diodes and / or switches (maximum break-down voltages are $600\,\mathrm{V}$ in the given system) and generate higher conduction losses than two-level converters, since each phase current is fed through two semiconductor devices, e.g. two IGBTs, with the sum of the voltage drops across two $600\,\mathrm{V}$ IGBTs being greater than the voltage drop across a single $1200\,\mathrm{V}$ IGBT [3]. T-type NPC converters, in comparison, allow for three-level operation at reduced conduction losses, since only a single diode or IGBT (again rated for $1200\,\mathrm{V}$) conducts the phase current to the positive or negative bus bar of the dc link [3]. Therefore, the T-type NPC inverter and rectifier topologies are very attractive regarding the investigated UPS system in order to achieve low conduction losses and reduced EMI filtering effort.

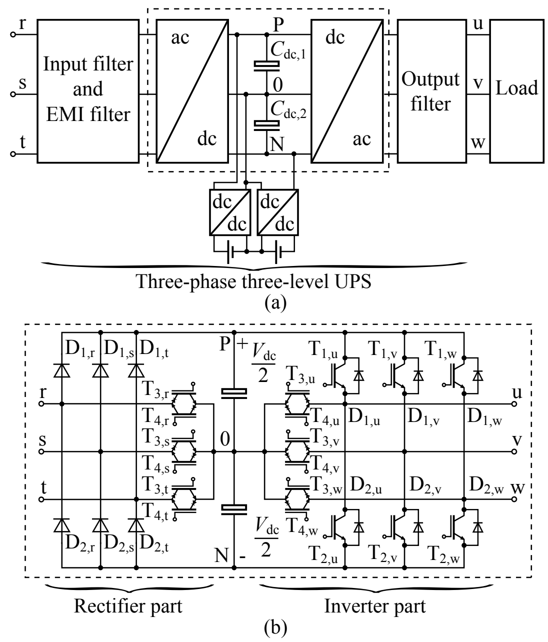

Fig. 1. (a) Proposed configuration of the three-phase three-level UPS system showing EMI filter, mains side rectifier, load side inverter, and dc–dc converters including backup batteries. (b) Schematic drawing of the power circuits of the mains side rectifier and the load side inverter; both, rectifier and inverter, employ 3LTTC topologies.

The T-type NPC converters require one bi-directional switch per phase, cf. Fig. 1(b). Bi-directional switches are typically realized with a common-emitter series connection of two IGBT / Free Wheeling Diode (FWD) modules as shown in Fig. 2(a) [3], [5]. As a consequence, two series connected semiconductor components, a diode and an IGBT, conduct the current through the bi-directional switch. In this context, reverse blocking IGBTs (RB-IGBTs) can be advantageously used to reduce the conduction losses of T-type rectifiers and inverters [6]–[8].

This paper details a comparison of the semiconductor losses of rectifier and inverter of the three-phase three-level UPS converter depicted in Fig. 1 for different realizations of the bi-directional switches, which includes realizations with RB-IGBTs and different types of conventional IGBT / FWD modules. The paper further investigates the improvements achieved with $1200\,\mathrm{V}$ SiC Schottky Barrier Diodes (SBDs) (instead of $1200\,\mathrm{V}$ Si rectifier diodes and FWDs) and $600\,\mathrm{V}$ SiC SBDs (instead of $600\,\mathrm{V}$ Si FWDs used in the bi-directional switches). **Section II** describes two realizations of the bi-directional switches, which are considered for loss comparison. **Section III** details the analytical semiconductor loss calculation models, i.e. conduction and switching loss models, for T-type rectifiers and inverters. **Section IV** presents measured switching losses, which are used to parameterize the switching loss model

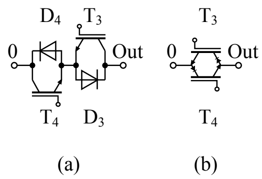

Fig. 2. Possible realizations of a bi-directional switch: (a) realization with conventional IGBTs and diodes, (b) realization with RB-IGBTs.

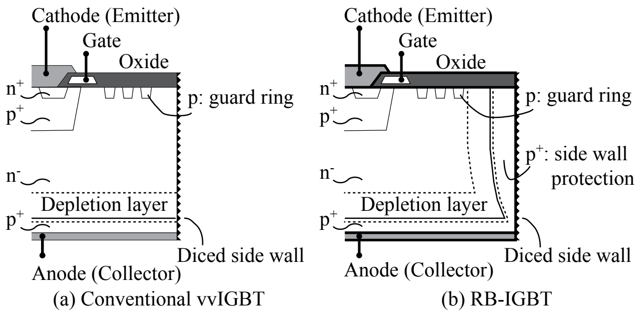

Fig. 3. (a) Internal structure of the conventional IGBT; (b) internal structure of the RB-IGBT for reverse voltage conditions. The reverse voltage forms the depletion layers shown in (a) and (b).

of Section III. Section IV further compares the losses and the total system efficiencies achieved with different realizations of the bi-directional switches, with and without SiC SBD, and for different switching frequencies.

II. Bi-directional power switch

A. Switch realizations

Fig. 2 shows two realizations of bi-directional switches with conventional IGBTs and FWDs or with RB-IGBTs. Further realizations of bi-directional switches, e.g. the realizations given in [2], [5], are expected to have higher or similar conduction losses than the realization of Fig. 2(a), and are, therefore, not considered in this comparison.

B. Internal structure of the RB-IGBT

The internal structures of a conventional IGBT and a RB-IGBT and the respective depletion layers under reverse voltage conditions are shown in Fig. 3. When a reverse voltage is applied to a conventional IGBT, the depletion layer extends from the backside anode (collector) towards the surface cathode (emitter). The depletion layer also extends to the diced side walls and causes high local electric fields, that are proportional to the reverse voltage. The semiconductor dicing process, however, unavoidably generates numerous crystal defects and mechanical imperfections at the diced side walls. The high local electric fields generate free carriers at these crystal defects causing the so-called leakage current fountain, which may irreversibly damage the IGBT [8].

The first concept of a RB-IGBT and the realization of its internal structure has been introduced in 2001 [6], [7]. Deep diffusion of a p^+-side wall protection at the diced side wall surface [cf. Fig. 3(b)] prevents the depletion layer from extending to the diced surface area of the IGBT under reverse voltage conditions. As a result, a huge reduction of the reverse leakage current under reverse voltage conditions is achieved.

Since the RB-IGBT and the conventional IGBT are only different with respect to the edge structures, same conduction and switching losses can be expected for both types of IGBTs if operated in forward direction. The RB-IGBT, however, shows a reverse recovery behavior similar to a rectifier diode if operated with reverse

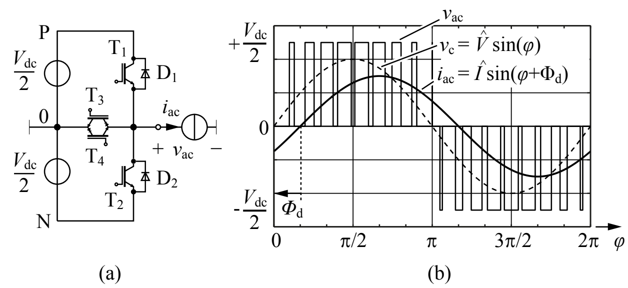

Fig. 4. (a) Single phase-leg of the 3LTTC converter; (b) general waveforms of input / output voltage and current for dedicated phase shift Φ_d, peak voltage $\hat{V}$, and peak current $\hat{I}$.

voltage, which causes the switching losses to increase and needs to be considered in the loss model detailed in the next section.

III. Analytical loss calculation model of T-type converters

A. Voltage and current waveforms at ac input / output side

Fig. 4(b) illustrates general input / output voltage and current waveforms of a single phase-leg of the 3LTTC converter at ac input / output side (e.g. mains input side or load output side), shown in Fig. 4(a). It is formed with two IGBTs (T_1 and T_2), two FWDs (D_1 and D_2) and two bi-directional switches (T_3 and T_4). In this paper, the multi-carrier pulse width modulation (PWM) scheme detailed in [9], [10] is considered. In Fig. 4(b), v_ac and i_ac are instantaneous input / output voltage and current of single phase-leg at ac side, respectively. v_c is the temporal average voltage of v_ac which is same with fundamental input voltage at mains side or output voltage at load side. $\varphi = \omega t$ denotes the phase of the fundamental voltage, Φ_d is the phase displacement between the fundamental components of current and voltage, $\hat{V}$ is the peak fundamental phase voltage, and $\hat{I}$ is the peak fundamental phase current. Thus, $\Phi_\mathrm{d} = 0^\circ$ denotes inverter mode of operation with unity power factor and $\Phi_\mathrm{d} = 180^\circ$ denotes rectifier mode of operation with unity power factor. Voltage and current amplitudes, $\hat{V}$ and $\hat{I}$, are defined from the modulation index M and the input / output apparent power S_ac as shown below.

$$\hat{V} = M\frac{V_\mathrm{dc}}{2} \quad (1)$$

$$\hat{I} = \frac{2}{3}\cdot\frac{S_\mathrm{ac}}{\hat{V}} \quad (2)$$

B. Conduction loss model

Fig. 5(a) shows a general on-state characteristicof an IGBT or a diode. Linearization of the characteristic, obtained at a given junction temperature T_j, yields the loss model parameters $V_\mathrm{f}(T_\mathrm{j})$ and $R_\mathrm{on}(T_\mathrm{j})$. The corresponding losses are calculated with the rms and the average currents through the device according to:

$$P_\mathrm{c} = R_\mathrm{on}(T_\mathrm{j})\, I^2_\mathrm{rms}(M,\hat{I},\Phi_\mathrm{d}) + + V_\mathrm{f}(T_\mathrm{j})\, I_\mathrm{avg}(M,\hat{I},\Phi_\mathrm{d}). \quad (3)$$

$R_\mathrm{on}(T_\mathrm{j})$ and $V_\mathrm{f}(T_\mathrm{j})$ denote temperature dependent on-state resistance and forward voltage drop values of the considered semiconductor, respectively. The temperature dependency is considered according to [11]:

$$R_\mathrm{on}(T_\mathrm{j}) = R_\mathrm{on}(T_\mathrm{j0})\left(\frac{T_\mathrm{j}}{T_\mathrm{j0}}\right)^{k_{\mathrm{R_{on}}}}, \quad (4)$$

$$V_\mathrm{f}(T_\mathrm{j}) = V_\mathrm{f}(T_\mathrm{j0})\left(\frac{T_\mathrm{j}}{T_\mathrm{j0}}\right)^{k_{\mathrm{V_f}}} \quad (5)$$

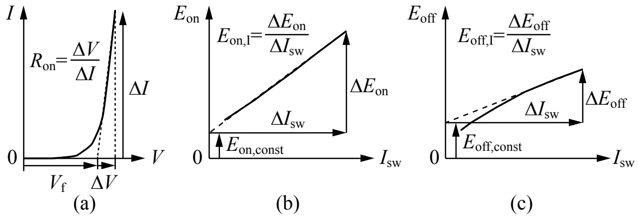

Fig. 5. (a) General on-state characteristics of IGBTs and diodes used to determine the parameters V_f and R_on of the conduction loss model. (b), (c) General illustration, how the parameters $E_\mathrm{on,const}$, $E_\mathrm{on,I}$, $E_\mathrm{off,const}$, and $E_\mathrm{off,I}$ of the switching loss model are extracted from the (b) turn-on and (c) turn off loss characteristics.

[T_j0 is the reference junction temperature in Kelvin; $R_\mathrm{on}(T_\mathrm{j0})$ and $V_\mathrm{f}(T_\mathrm{j0})$ are on-state resistance and forward voltage drop at the reference junction temperature]. The temperature coefficients $k_{\mathrm{R_{on}}}$ and $k_{\mathrm{V_f}}$ of all considered devices, determined with data sheet values and least mean square approximation, are listed in Tab. IV.

The analytical expressions of average and rms currents through all devices are derived according to [9]. The currents through the IGBTs with a suggested break-down voltage of 1200 V, i.e. the two IGBTs T_1 and T_2 in Fig. 4, are:

$$I_\mathrm{avg,T12} = \frac{\hat{I}M\,(\pi-\Phi_\mathrm{d})\cos(\Phi_\mathrm{d})}{4\pi} + \frac{\sin(\Phi_\mathrm{d})}{4\pi}, \tag{6}$$

$$I_\mathrm{rms,T12} = \hat{I}\left[\cos\left(\frac{\Phi_\mathrm{d}}{2}\right)\right]^2\sqrt{\frac{2M}{3\pi}}; \tag{7}$$

the currents through D_1 and D_2 (or the FWD of T_1 and T_2) are:

$$I_\mathrm{avg,D12} = \frac{\hat{I}M\,[\sin(\Phi_\mathrm{d})-\Phi_\mathrm{d}\cos(\Phi_\mathrm{d})]}{4\pi}, \tag{8}$$

$$I_\mathrm{rms,D12} = \hat{I}\left[\sin\left(\frac{\Phi_\mathrm{d}}{2}\right)\right]^2\sqrt{\frac{2M}{3\pi}}; \tag{9}$$

and the currents in each IGBT of the bi-directional switch (and in the IGBTs' FWD, if applicable), i.e. T_3 and T_4, are:

$$I_\mathrm{avg,T34} = \frac{2\hat{I}+\hat{I}M\left(\Phi_\mathrm{d}-\frac{\pi}{2}\right)\cos(\Phi_\mathrm{d})}{2\pi} + \frac{(-1)\hat{I}M\sin(\Phi_\mathrm{d})}{2\pi}, \tag{10}$$

$$I_\mathrm{rms,T34} = \hat{I}\sqrt{\frac{3\pi-2M\,[3+\cos(2\Phi_\mathrm{d})]}{12\pi}}. \tag{11}$$

These equations are valid for both inverter and rectifier mode of operations ($0° \leq \Phi_\mathrm{d} \leq 180°$).

C. Switching loss model

The switching states of a single leg of the 3LTTC, except for transient states during dead time intervals, are listed in Tab. I. The current commutation paths related to the switching states and the input / output current conditions are shown in Fig. 6. Tab. II summarizes the expressions for the switching loss energies that result for different state transitions.

Fig. 7 serves as a basis for explaining the switching operations present in the given 3LTTC converter. It depicts the considered waveform of $v_\mathrm{ac}(t)$ and two switching operations for inverter mode of operation in Fig. 7(a), at $t = t_\mathrm{a}$ ($\mathrm{S}_{1001} \rightarrow \mathrm{S}_{0011}$) and $t = t_\mathrm{b}$ ($\mathrm{S}_{0011} \rightarrow \mathrm{S}_{1001}$); positive and approximately constant input / output current is assumed. The states involved in both depicted switching operations are, thus, S_{1001} and S_{0011} and, according to Tab. I,

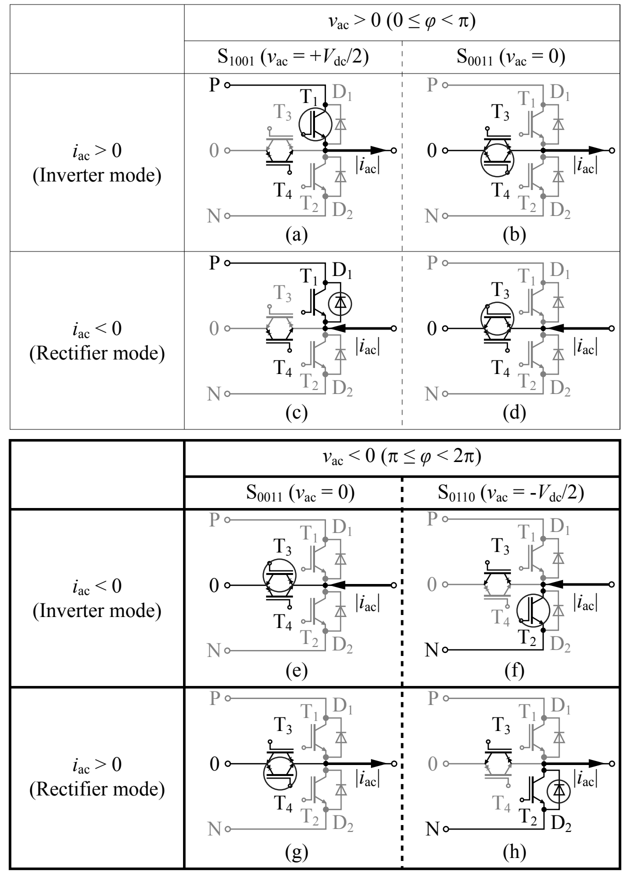

Fig. 6. Current commutation mode, the encircled device conducts current.

the gate signals of the switches T_1 and T_3 need to be changed. The switch T_3, however, is operated with reverse voltage and, for $v_\mathrm{ac}(t) = 0$ and $i_\mathrm{ac}(t) > 0$, T_4 takes over the input / output current, cf. Fig. 6(b).

Fig. 7(b) and Fig. 7(c) depict the emitter to collector voltage (blue) and collector current (red) waveforms measured at $t = t_\mathrm{a}$ for T_1 and T_4, which are used to determine the switching losses. T_1 effectively turns off at $t = t_\mathrm{a1}$ [Fig. 7(b)]; the clearly visible tail current largely contributes to the total turn-off losses $E_\mathrm{off,T12}$,

$$E_\mathrm{off,T12} = \int_{t\mathrm{a1}}^{t\mathrm{a2}} i_\mathrm{c,T12}(t)\cdot v_\mathrm{ce,T12}(t)\;\mathrm{d}t. \tag{12}$$

The turn-on losses of T_4, Fig. 7(c), are negligible.

Fig. 7(d) and (e) show emitter to collector voltages (blue) and collector currents (red) of T_1 and T_4 at $t = t_\mathrm{b}$. The switch T_1 turns on at $t = t_\mathrm{b1}$, which causes the collector current of T_3 to fall. T_3's collector current is zero at $t = t_\mathrm{b2}$, and, subsequently, gets negative due to reverse recovery effects. At $t = t_\mathrm{b3}$ the collector current reaches the maximum reverse recovery current I_rrm. Fig. 7(e), thus, shows the reverse recovery behavior of T_4, i.e. the RB-IGBT FGW85N60RB. The reverse recovery charge obtained from this figure, $Q_\mathrm{rs} + Q_\mathrm{rf} \approx 6.5\,\mu\mathrm{C}$, causes reverse recovery losses of T_4 during $t_\mathrm{b2} < t < t_\mathrm{b5}$. Moreover, the reverse recovery behavior of T_4 causes a high temporary collector current in T_1, which increases the turn-on losses of T_1, as can be seen in Fig. 7(d). The turn-on losses $E_\mathrm{on,T12}$ and the reverse recovery losses $E_\mathrm{rr,T34}$ are evaluated with:

$$E_\mathrm{on,T12} = \int_{t\mathrm{b1}}^{t\mathrm{b4}} i_\mathrm{c,T12}(t)\cdot v_\mathrm{ce,T12}(t)\;\mathrm{d}t, \tag{13}$$

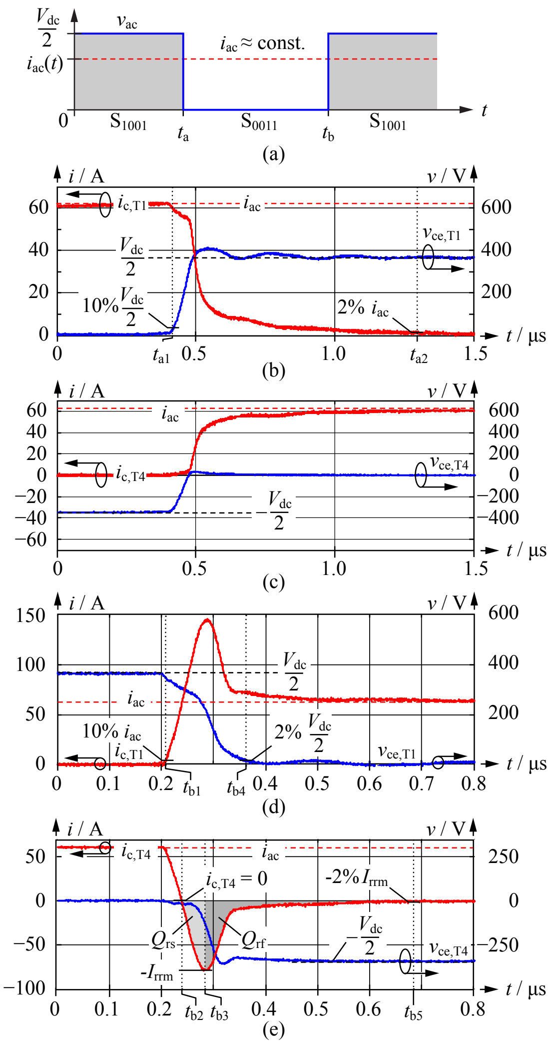

Fig. 7. Transient collector to emitter voltages and collector currents during switching, obtained for $v_{ac}(t) \geq 0$ and $i_{ac}(t) > 0$ (inverter mode of operation): (a) simplified illustration of the considered input / output voltage and current waveforms showing the considered switching instants t_a and t_b; (b) and (c) waveforms measured for (b) T_1 and (c) T_4 during turn-off of T_1 at $t = t_a$; (d) (e) waveforms measured for (d) T_1 and (e) T_4 during turn-on of T_1 at $t = t_b$; blue curves: collector to emitter voltages, red curves: collector currents. Selected operating point: $V_{dc} = 720\,\mathrm{V}$, $i_{ac} = 60\,\mathrm{A} \approx$ constant. Employed semiconductor switches: T_1 and T_2: FGW40N120HD, T_3 and T_4: FGW85N60RB.

$$E_{rr,T34} = \int_{tb2}^{tb5} i_{c,T34}(t) \cdot v_{ce,T34}(t)\ dt. \tag{14}$$

Turn-off and turn-on losses of each IGBT and the reverse recovery losses of the corresponding RB-IGBT (or FWD in case of conventional IGBT / FWD modules being used) are calculated according to [3] and as shown below.

$$\begin{aligned} P_{sw,off} &= f_{sw}\left[E_{off,I}\left(V_{dc}, T_j\right) I_{sw,avg}\left(\hat{I}_{ac}, \Phi_d\right) + \right. \\ &\quad \left. E_{off,const}\left(V_{dc}, T_j\right) D_{d,sw}\left(\Phi_d\right)\right] \end{aligned} \tag{15}$$

$$\begin{aligned} P_{sw,on} &= f_{sw}\left[E_{on,I}\left(V_{dc}, T_j\right) I_{sw,avg}\left(\hat{I}_{ac}, \Phi_d\right) + \right. \\ &\quad \left. E_{on,const}\left(V_{dc}, T_j\right) D_{d,sw}\left(\Phi_d\right)\right] \end{aligned} \tag{16}$$

$$\begin{aligned} P_{sw,rr} &= f_{sw}\left[E_{rr,I}\left(V_{dc}, T_j\right) I_{sw,avg}\left(\hat{I}_{ac}, \Phi_d\right) + \right. \\ &\quad \left. E_{rr,const}\left(V_{dc}, T_j\right) D_{d,sw}\left(\Phi_d\right)\right] \end{aligned} \tag{17}$$

TABLE I. SWITCHING STATES

	Switching states		
	S_{1001}	S_{0011}	S_{0110}
T_1:	on	off	off
T_2:	off	off	on
T_3:	off	on	on
T_4:	on	on	off
v_{ac}:	$+V_{dc}/2$	0	$-V_{dc}/2$

The turn-on losses of the FWDs are neglected in this paper. $I_{sw,avg}$ denotes the averaged switching current over single fundamental period, D_{sw} is the normalized period the device acts as a switch, and f_{sw} is the switching frequency. Analytical expressions for the average switching current are given in [12] and summarized below.

$$I_{sw,avg,T12} = \hat{I}_{ac}\left[\frac{1+\cos\left(\Phi_d\right)}{2\pi}\right], \tag{18}$$

$$D_{sw,T12} = \frac{\pi - \Phi_d}{2\pi}, \tag{19}$$

$$I_{sw,avg,D12} = \hat{I}_{ac}\left\{\frac{\left[\sin\left(\frac{\Phi_d}{2}\right)\right]^2}{\pi}\right\}, \tag{20}$$

$$D_{sw,D12} = \frac{\Phi_d}{2\pi}, \tag{21}$$

$$I_{sw,avg,D34} = I_{sw,avg,T12}, \tag{22}$$

$$D_{sw,D34} = D_{sw,T34}, \tag{23}$$

$$I_{sw,avg,T34} = I_{sw,avg,D12}, \tag{24}$$

$$D_{sw,T34} = D_{sw,D12}. \tag{25}$$

$I_{sw,avg,T34}$ is the average switching current of T_3 and T_4 when the devices are operated as IGBTs (e.g. switching in rectifier mode of operation) and $I_{sw,avg,D34}$ is the average switching current of T_3 and T_4 when the devices are operated as FWDs (e.g. switching in inverter mode of operation). The same notation is used for $D_{sw,T34}$ and $D_{sw,D34}$. These equations are valid for both inverter and rectifier mode of operations ($0^\circ \leq \Phi_d \leq 180^\circ$). The six coefficients needed to calculate the switching losses, $E_{off,I}$, $E_{off,const}$, $E_{on,I}$, $E_{on,const}$, $E_{rr,I}$, and $E_{rr,const}$, are extracted as shown in Fig. 5(b) and (c) from device's data sheet or measurement results. The impact of the dc bus voltage, V_{dc}, and the junction temperature, T_j, is considered according to [11]:

$$E_{off,I} = E_{off,I,V_0,T_{j0}}\left(\frac{V_{dc}}{V_{dc0}}\right)\left(\frac{T_j}{T_{j0}}\right)^{k_{E_{off}}}, \tag{26}$$

$$E_{off,const} = E_{off,const,V_0,T_{j0}}\left(\frac{V_{dc}}{V_{dc0}}\right)\left(\frac{T_j}{T_{j0}}\right)^{k_{E_{off}}}, \tag{27}$$

$$E_{on,I} = E_{on,I,V_0,T_{j0}}\left(\frac{V_{dc}}{V_{dc0}}\right)\left(\frac{T_j}{T_{j0}}\right)^{k_{E_{on}}}, \tag{28}$$

$$E_{on,const} = E_{on,const,V_0,T_{j0}}\left(\frac{V_{dc}}{V_{dc0}}\right)\left(\frac{T_j}{T_{j0}}\right)^{k_{E_{on}}}, \tag{29}$$

$$E_{rr,I} = E_{rr,I,V_0,T_{j0}}\left(\frac{V_{dc}}{V_{dc0}}\right)\left(\frac{T_j}{T_{j0}}\right)^{k_{E_{rr}}}, \tag{30}$$

$$E_{rr,const} = E_{rr,const,V_0,T_{j0}}\left(\frac{V_{dc}}{V_{dc0}}\right)\left(\frac{T_j}{T_{j0}}\right)^{k_{E_{rr}}}. \tag{31}$$

Here, $V_{dc0} = 720\,\mathrm{V}$ is the voltage and $T_{j0} = (273.15 + 150)\,\mathrm{K}$ is the junction temperature at which the measurements have been conducted.

D. Estimating the increase of the turn-on loss energy due to the reverse recovery charge of FWDs

Most of the results presented in Section IV are solely based on experimental results, only the losses of the two converter

TABLE II. SWITCHING LOSS ENERGIES

Input / output current condition	Switching transitions	
	$S_{0011} \rightarrow S_{1001}$	$S_{1001} \rightarrow S_{0011}$
$i_{ac} > 0$	$E_{on,T12}$ + $E_{rr,T34}$	$E_{off,T12}$
$i_{ac} < 0$	$E_{off,T34}$	$E_{on,T34}$ + $E_{rr,D12}$

Input / output current condition	Switching transitions	
	$S_{0110} \rightarrow S_{0011}$	$S_{0011} \rightarrow S_{0110}$
$i_{ac} > 0$	$E_{on,T34}$ + $E_{rr,D12}$	$E_{off,T34}$
$i_{ac} < 0$	$E_{off,T12}$	$E_{on,T12}$ + $E_{rr,T34}$

configurations which use conventional IGBTs with anti-parallel SiC SBD C3D20060D for the bi-directional switch (configurations B3 and C3 in Section IV) are estimated.

According to Section III-C the amount of reverse recovery charge, $Q_{rr} = Q_{rs} + Q_{rf}$, of the FWD (or RB-IGBT) has a strong impact on the resulting turn-on losses. Thus, the turn-on switching losses available in data sheets are not readily applicable for the presented comparison, since the T-type inverter employs different types of power semiconductor switches, i.e. T_1 and T_2 are conventional IGBT / FWD modules with $V_{(BR)CES} = 1200\,V$ and T_3 and T_4 are RB-IGBTs with $V_{(BR)CES} = 600\,V$.

The expected turn-on losses can be estimated based on [13] using the transient voltage and current waveforms during turn-on depicted in Fig. 7(d) and (e). According to [13] the turn-on losses of the IGBT, $E_{on,T}$, can be separated into two parts. The first part denotes the turn-on losses without reverse recovery,

$$E_{on,T,0} = E_{on,T} - \Delta E_{on,T}, \tag{32}$$

and the second part denotes additional losses due to reverse recovery,

$$\Delta E_{on,T} \approx (t_s i_{ac} + Q_{rs}) \frac{V_{dc}}{2}, \tag{33}$$

t_s is the delay time due to reverse recovery,

$$t_s = t_{b3} - t_{b2}. \tag{34}$$

$E_{on,T,0}$ is calculated based on measurement results, then the turn-on losses with SiC SBDs instead of Si FWDs (configurations B3 and C3 in Section IV) are estimated with (32) as below.

$$\tilde{E}_{on,T} = E_{on,T,0} + \Delta \tilde{E}_{on,T}, \tag{35}$$

and the second part denotes estimated additional losses due to the total capacitive charge Q_c from SiC SBDs,

$$\Delta \tilde{E}_{on,T} = \left(\tilde{t}_s i_{ac} + Q_c\right) \frac{V_{dc}}{2}, \tag{36}$$

$\tilde{t}_s$ is the estimated delay time due to Q_c,

$$\tilde{t}_s = \sqrt{\frac{2Q_c}{i'_{c,T}(t_{b2})}}, \tag{37}$$

$i'_{c,T}(t_{b2})$ is a derivative value of collector current at $t = t_{b2}$ and measurement results are used for this value. $Q_c = 16\,nC$ at reverse voltage $V_r = 360\,V$ is obtained from the data sheet of C3D20060D.

E. Thermal model

The temperature of each semiconductor's junction is calculated based on the conduction and switching losses, P_c and P_{sw}, of the considered switch and with a simplified linear thermal model, which considers the thermal resistance from junction to case, $R_{th,j-c}$:

$$T_j = R_{th,j-c} \cdot (P_c + P_{sw}) + T_{case} \tag{38}$$

Conduction losses and switching losses show a non-linear temperature dependency. Hence, an iterative procedure is implemented to solve for junction temperature, conduction losses, and switching losses.

TABLE IV. EXTRACTED CONDUCTION LOSS MODEL PARAMETERS

Name	T_{j0}[°C]	$V_{f,T_{j0}}$[V]	$R_{on,T_{j0}}$[Ω]	k_{V_f}	$k_{R_{on}}$
IGBT1(T)	175	1.04	0.016	0.0565	1.22
IGBT1(D)	175	0.86	0.016	-1.1163	0.288
SBD1	150	0.75	0.037	-0.6346	1.824
IGBT2	150	1.06	0.018	-0.3373	0.55
IGBT3(T)	150	1.02	0.021	0.0838	1.108
IGBT4(T)	150	0.76	0.02	-0.3044	1.155
IGBT3(D)	150	1.01	0.018	-1.5906	-0.819
IGBT4(D)	Same as IGBT3(D)				
SBD2	175	0.72	0.065	-0.6061	1.989

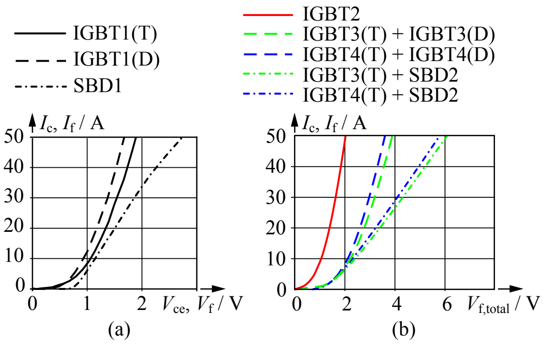

Fig. 8. On-state forward voltage drop versus collector or forward current at $T_j = 150\,°C$, (a) for switches with $V_{(BR)CES} = 1200\,V$ and (b) for bi-directional switches, cf. Fig. 2, with $V_{(BR)CES} = 600\,V$.

IV. COMPARISON OF T-TYPE CONVERTERS WITH AND WITHOUT RB-IGBTS

A. IGBT / FWD modules suitable for comparison

Different types of IGBTs are considered for the bi-directional switch, including devices optimized with respect to low conduction losses or low switching losses, in order to allow for a meaningful comparison of the losses obtained with conventional IGBTs and RB-IGBTs. Tab. III lists the considered devices:

- IGBT1: 1200 V IGBT + FWD for T_1, T_2, D_1 and D_2 ,
- IGBT2: 600 V RB-IGBT for T_3 and T_4 ,
- IGBT3 / IGBT4: two 600 V IGBT + FWD for T_3 and T_4 ,
- SBD1: 1200 V SiC SBD for D_1 and D_2 ,
- SBD2: 600 V SiC SBD for T_3 and T_4 .

Two parallel connected components IGBT1 are considered in order to achieve reduced conduction losses and, thus, the total maximum forward currents of D_1 and D_2 are 60 A. In order to save costs, the rated currents of the selected SiC SBDs (SBD1 and SBD2) are approximately two thirds of the rated currents of the Si FWDs. With this, the diode currents are still well below the rated diode currents, however, considerably increased conduction losses result.

B. Parameterization of the conduction loss models

The conduction loss model is parameterized with data sheet values based on least mean square approximation, the obtained coefficients are listed in Tab. IV. There, IGBT(T) denotes the IGBT and IGBT(D) the FWD if a single package contains both, IGBT and FWD. Fig. 8 depicts the forward characteristics of the considered devices.

C. Switching losses measurement results

During switching, a device with a breakdown voltage of 1200 V and a second device with $V_{(BR)CES} = 600\,V$ are operated together,

TABLE III. CONSIDERED SEMICONDUCTOR DEVICES FOR LOSS COMPARISON; $V_{(\mathrm{BR})\mathrm{CES}}$: MAXIMUM COLLECTOR-EMITTER VOLTAGE OF IGBTS; V_{RRM}: REPETITIVE PEAK REVERSE VOLTAGE OF FWDS; I_{C}: MAXIMUM DC COLLECTOR CURRENT OF IGBTS; I_{F}: AVERAGE FORWARD CURRENT OF FWDS; N_{p}: THE NUMBER OF PARALLELED MODULES.

Name	Device type	$V_{(\mathrm{BR})\mathrm{CES}}$, V_{RRM}	I_{C}, I_{F}	$R_{\mathrm{th,j-c,T}}$ / $R_{\mathrm{th,j-c,D}}$	N_{p}	Model number	Manufacture
IGBT1	Si IGBT and FWD	1200	40 / 30	0.439 / 0.781	2	FGW40N120HD	Fuji Electric
SBD1	SiC SBD	1200	18	0.63	2	FDCW18S120	Fuji Electric
IGBT2	Si RB-IGBT	600	85	0.208	1	FGW85N60RB	Fuji Electric
IGBT3	Si IGBT and FWD	600	75 / 30	0.21 / 0.9	1	IXXH75N60C3D1	IXYS
IGBT4	Si IGBT and FWD	600	75 / 30	0.21 / 0.9	1	IXXH75N60B3D1	IXYS
SBD2	SiC SBD	600	20	0.55	1	C3D20060D	CREE

TABLE V. COMBINATION OF SWITCHING DEVICES FOR COMPARISON.

Label	1200 V IGBT for T_1 and T_2	1200 V FWD for D_1 and D_2	600 V IGBT for T_3 and T_4	600 V FWD for D_3 and D_4
A1	Si IGBT (IGBT1(T))	Si FWD (IGBT1(D))	Si RB-IGBT (IGBT2)	Si RB-IGBT (IGBT2)
B1	Si IGBT (IGBT1(T))	Si FWD (IGBT1(D))	Si IGBT (IGBT3(T))	Si FWD (IGBT3(D))
C1	Si IGBT (IGBT1(T))	Si FWD (IGBT1(D))	Si IGBT (IGBT4(T))	Si FWD (IGBT4(D))
A2	Si IGBT (IGBT1(T))	SiC SBD (SBD1)	Si RB-IGBT (IGBT2)	Si RB-IGBT (IGBT2)
B2	Si IGBT (IGBT1(T))	SiC SBD (SBD1)	Si IGBT (IGBT3(T))	Si FWD (IGBT3(D))
C2	Si IGBT (IGBT1(T))	SiC SBD (SBD1)	Si IGBT (IGBT4(T))	Si FWD (IGBT4(D))
B3	Si IGBT (IGBT1(T))	SiC SBD (SBD1)	Si IGBT (IGBT3(T))	SiC SBD (SBD2)
C3	Si IGBT (IGBT1(T))	SiC SBD (SBD1)	Si IGBT (IGBT4(T))	SiC SBD (SBD2)

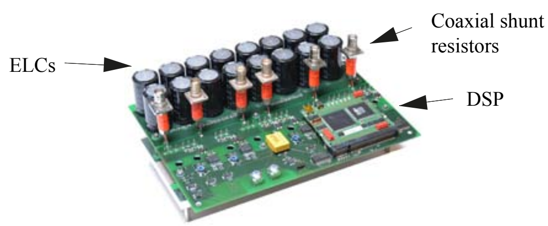

Fig. 9. The switching loss measurement setup.

cf. Section III, and, according to Tab. II, the resulting switching losses depend on the used combination of switches. With the considered IGBTs and SiC SBDs the eight different combinations of devices listed in Tab. V are feasible. The switching losses resulting from the first six combinations, A1, B1, C1, A2, B2 and C2 are measured with the switching loss measurement setup depicted in Fig. 9 and for the conditions listed below.

- Employed dc link voltage: $V_{\mathrm{dc}} = 720\,\mathrm{V}$.
- Junction temperatures: $T_{\mathrm{j}} = 30\,°\mathrm{C}$, $T_{\mathrm{j}} = 150\,°\mathrm{C}$.
- Gate resistance: $R_{\mathrm{G}} = 5.1\,\Omega$.
- On- and off-state gate voltages: $V_{\mathrm{GE,on}} = 16\,\mathrm{V}$, $V_{\mathrm{GE,off}} = -6\,\mathrm{V}$.

The switching losses obtained for the remaining combinations B3, and C3 are estimated with (35).

The resulting switching losses are shown in Fig. 10 for all considered device combinations. The extracted parameters of the switching loss model are listed in Tab. VI.

1) Rectifier mode of operation: The turn-on losses of T_3 and T_4, $E_{\mathrm{on,T34}}$, and the reverse recovery losses of the FWDs of D_1 and D_2, $E_{\mathrm{rr,D12}}$, largely depend on the reverse recovery behavior of the FWDs of D_1 and D_2. Therefore, as shown in Fig. 10(b) and (c), $E_{\mathrm{on,T34}}$ and $E_{\mathrm{rr,D12}}$ are similar for the device combinations A1, B1, and C1 and can be considerably reduced with SiC SBDs (combinations A2, B2, C2, A3, and B3), i.e. the type of IGBT used for T_3 and T_4 has only little influence on the achieved turn-on losses. The IGBT selected for T_3 and T_4 mainly determines the obtained turn-off losses, cf. Fig. 10(a): it is seen that the IBGT optimized for speed yields minimum switching losses (e.g. B1), maximum switching losses result with the IGBT optimized for low conduction losses (e.g. C1), and the losses obtained with the considered RB-IGBT are in between (e.g. A1).

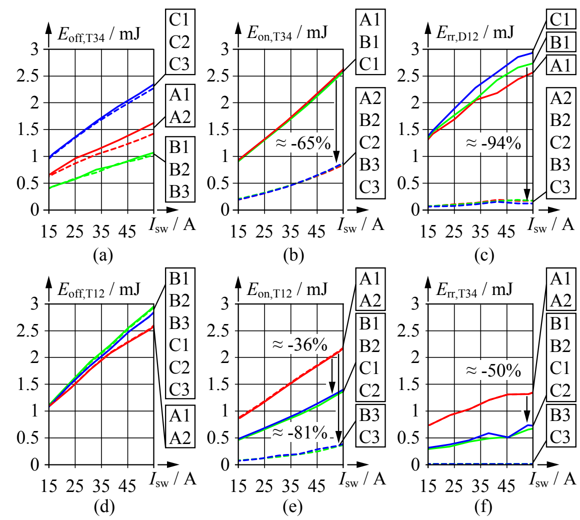

Fig. 10. Switching losses measured (A1, A2, A3) or estimated (B1, B2, B3, C2, C3) for the different considered device combinations, different switch currents I_{sw}, $V_{\mathrm{dc}} = 720\,\mathrm{V}$, and $T_{\mathrm{j}} = 150\,°\mathrm{C}$: (a), (b) and (c) denote the switching losses for rectifier mode of operation and (d), (e) and (f) the switching losses for inverter mode of operation.

2) Inverter mode of operation: The turn-on losses of T_1 and T_2, $E_{\mathrm{on,T12}}$, and the reverse recovery losses of T_3 and T_4 (or the FWDs of T_3 and T_4 in case of conventional IGBTs being used), $E_{\mathrm{rr,T34}}$, mainly depend on the devices considered for T_3 and T_4. Thus, due to comparably high reverse recovery charges of the RB-IGBTs, the values for $E_{\mathrm{on,T12}}$ and $E_{\mathrm{rr,T34}}$, are considerably higher for the configurations A1 and A2 than for the configurations using conventional IGBT / FWD modules (B1, B2, B3, C2, and C3), since the use of faster and smaller chips allows for a reduction of the reverse recovery charge of the employed FWDs. The turn-off losses of T_1 and T_2, $E_{\mathrm{off,T12}}$ are to a large part caused by the tail currents of T_1 and T_2 and are nearly independent of the type of IGBT selected for T_3 and T_4.

D. Loss comparison results and discussion

The total semiconductor losses of three-phase 3LTTC with and without the RB-IGBT are analyzed. In Fig. 11(a) and (b), total semiconductor losses of the 3LTTC are presented for operation in the switching frequency range of 5 kHz to 35 kHz for rectifier and inverter mode of operations, respectively.

TABLE VI. Parameter values of the switching loss models for the different considered device combinations being determined for $V_{\mathrm{dc0}} = 720\,\mathrm{V}$ and $T_{\mathrm{j0}} = 150\,°\mathrm{C}$.

	600 V IGBT (T_3 and T_4)						1200 V FWD (D_1 and D_2)		
	$E_{\mathrm{off,I}}$[mJ/A]	$E_{\mathrm{off,const}}$[mJ]	$k_{E_{\mathrm{off}}}$	$E_{\mathrm{on,I}}$[mJ/A]	$E_{\mathrm{on,const}}$[mJ]	$k_{E_{\mathrm{on}}}$	$E_{\mathrm{rr,I}}$[mJ/A]	$E_{\mathrm{rr,const}}$[mJ]	$k_{E_{\mathrm{rr}}}$
A1	0.02	0.239	2.123	0.038	0.234	1.259	0.019	0.557	3.573
B1	0.014	0.139	1.192	0.035	0.221	1.416	0.023	0.559	3.139
C1	0.03	0.417	1.006	0.036	0.235	1.331	0.024	0.581	3.434
A2	0.016	0.257	2.448	0.017	-0.083	-0.026	0.003	0.083	0.024
B2	0.014	0.149	1.191	0.016	-0.092	-0.423	0.003	0.072	-0.184
C2	0.029	0.424	1.013	0.017	-0.094	0.146	0.002	0.078	-0.477
B3	Same as B2			Same as B2			Same as B2		
C3	Same as C2			Same as C2			Same as C2		

	1200 V IGBT (T_1 and T_2)						600 V Diode (T_3 and T_4)		
	$E_{\mathrm{off,I}}$[mJ/A]	$E_{\mathrm{off,const}}$[mJ]	$k_{E_{\mathrm{off}}}$	$E_{\mathrm{on,I}}$[mJ/A]	$E_{\mathrm{on,const}}$[mJ]	$k_{E_{\mathrm{on}}}$	$E_{\mathrm{rr,I}}$[mJ/A]	$E_{\mathrm{rr,const}}$[mJ]	$k_{E_{\mathrm{rr}}}$
A1	0.038	0.563	0.598	0.032	0.364	1.767	0.013	0.418	1.779
B1	0.046	0.371	0.919	0.021	0.11	2.396	0.008	0.08	2.424
C1	0.045	0.383	0.929	0.022	0.121	1.946	0.009	0.141	1.85
A2	Same as A1			Same as A1			Same as A1		
B2	Same as B1			Same as B1			Same as B1		
C2	Same as C1			Same as C1			Same as C1		
B2	0.045	0.364	0.919	0.006	-0.017	2.067	0	0	0
C2	0.044	0.376	0.929	0.007	-0.026	0.742	0	0	0

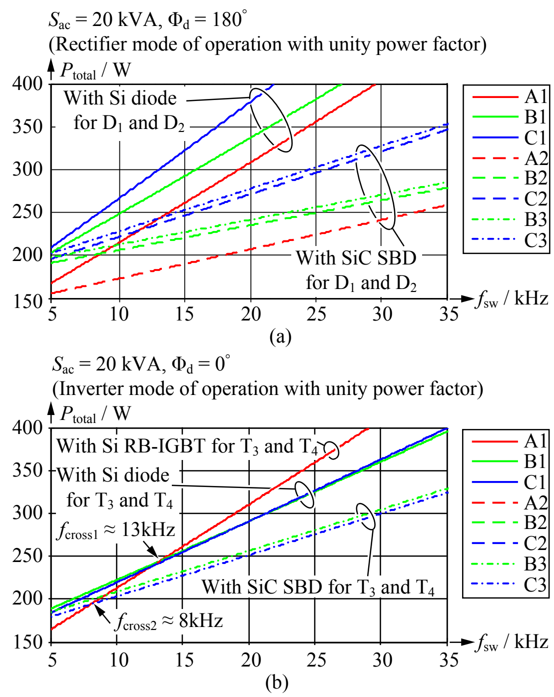

Fig. 11. Total loss comparison of three phase 3LTTCs for the eight different device combinations listed in Tab. V operation with unity power factor, $\hat{V} = 325\,\mathrm{V}$ and $\hat{I} = 41\,\mathrm{A}$: (a) result for rectifier mode of operation ($\Phi_{\mathrm{d}} = 180\,°$) and (b) for inverter mode of operation ($\Phi_{\mathrm{d}} = 0\,°$). f_{cross1} is the crossover frequency for total losses regarding A1 and B1 (or A1 and C1), f_{cross2} is the crossover frequency of A1 and B3 (or A1 and C3

In rectifier mode of operation, Fig. 11(a), the configuration with RB-IGBTs, A1, shows lower total losses than B1 and C1, mainly because T_3 and T_4 generate no reverse recovery effects in rectifier mode of operation and, thus, the reduced conduction losses of the bi-directional switch formed with RB-IGBTs directly facilitates lower total losses. A detailed inspection reveals that configuration B1 generates lower total switching losses than A1 which yields lowest total losses configuration B1 at very high switching frequencies, $f_{\mathrm{sw}} > 69.4\,\mathrm{kHz}$. There, however, exceedingly high total losses of more than 800 W render these solutions less suitable. Further total loss reduction is achieved with SiC SBDs being used for D_1 and D_2. Due to zero reverse recovery charge from D_1 and D_2, large switching loss reductions of $E_{\mathrm{rr,D12}}$ and $E_{\mathrm{off,T34}}$ are achieved as shown in Fig. 10(b) and (c). Again, the configuration with RB-IGBTs, A2, also features lower total losses than configurations B2 and C2 (up to 71 kHz) because of the reduced conduction losses achieved with the RB-IGBTs. No improvements are achieved with configurations B3 and C3 (SiC SBD in parallel to conventional IGBTs T_3 and T_4) in rectifier mode of operation, since the FWDs of T_3 and T_4 generate no reverse recovery effects.

In inverter mode of operation, configuration A1 allows for lower total losses than configurations B1 and C1 for switching frequencies up to 13 kHz in Fig. 11(b). In inverter mode of operation T_3 and T_4 are subject to reverse recovery effects, which causes increased total losses of configuration A1, i.e. configuration A1 shows higher values of $E_{\mathrm{rr,T34}}$ and $E_{\mathrm{on,T12}}$ than configurations B1 and C1, cf. Fig. 10(e) and (f). In inverter mode of operation, with unity power factor, the diodes D_1 and D_2 do not contribute to the switching losses and, therefore, the losses calculated for the configurations A2, B2, and C2, i.e. D_1 and D_2 are realized with SiC SBDs, are similar to the losses calculated for the configurations A1, B1, and C1, respectively. Further total loss reduction are calculated for configurations B3 and C3 (SiC SBDs used for the FWDs of T_3 and T_4) for switching frequencies greater than 8 kHz due to zero reverse recovery charge from these SiC SBDs.

Fig. 12 depicts the loss distributions (conduction and switching losses of all IGBTs and diodes) for assumed total semiconductor losses of 500 W, which would yield an efficiency of 97.5 %. These losses are equally distributed to rectifier and inverter, i.e. 250 W each. Fig. 12 further shows the switching frequency achieved for the assumed total semiconductor losses and for the different configurations. In rectifier mode of operation, Fig. 12(a), configuration A1 shows lower total conduction losses and higher operating switching frequency of 13.9 kHz than configurations B1 (10.3 kHz) and C1 (8.7 kHz). Higher switching frequencies are achieved if D_1 and D_2 are replaced by SiC SBDs, i.e. with configurations A2 (32.5 kHz), B2 (25.2 kHz), and C2 (15.8 kHz). There, the total conduction losses are slightly higher than for configurations A1, B1, and C1 due to increased conduction losses of SiC SBDs, however, the total switching losses are reduced due to zero reverse recovery charge from D_1 and D_2. Configurations B3 and C3 show higher conduction losses due to the SiC SBDs that are used to realize the bi-directional switch; no further reduction of the switching losses is achieved, though. Therefore, the operating switching frequencies are lower than for configurations B2 and C2. Thus, for rectifier mode of operation and assumed semiconductor losses of 250 W, configurations A2, i.e. the use of SiC SBDs for D_1 and D_2 and RB-IGBTs, features the highest switching frequency.

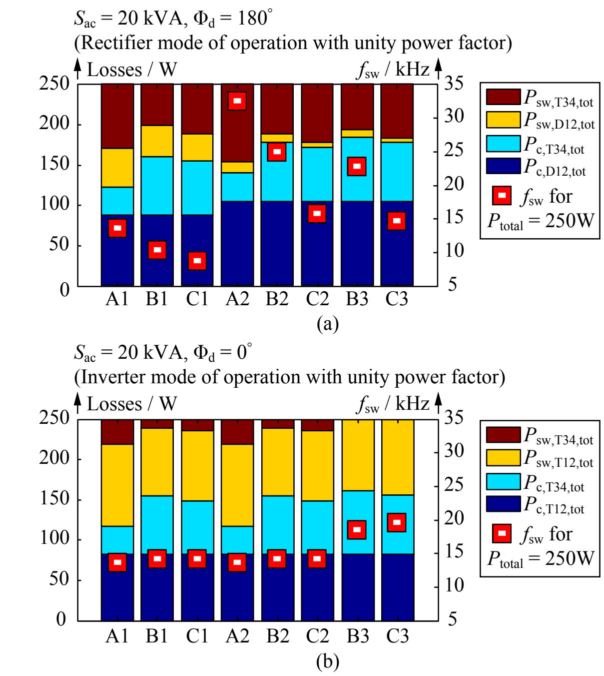

Fig. 12. Total conduction and switching loss distributions of three phase 3LTTC for the eight different configurations listed in Tab. V and for operation with fixed total loss $P_{\mathrm{total}} = 250\,\mathrm{W}$, unity power factor, $\hat{V} = 325\,\mathrm{V}$ and $\hat{I} = 41\,\mathrm{A}$: (a) results for rectifier mode of operation ($\Phi_{\mathrm{d}} = 180\,°$) and (b) inverter mode of operation ($\Phi_{\mathrm{d}} = 0\,°$). The red marks show the operating switching frequencies determined for fixed total loss. $P_{c,T12,tot}$, $P_{c,D12,tot}$ and $P_{c,T34,tot}$ denote the total conduction losses of T_1 and T_2, D_1 and D_2, and T_3 and T_4 (including the FWDs of T_3 and T_4, if applicable), respectively. $P_{\mathrm{sw,T12,tot}}$, $P_{\mathrm{sw,D12,tot}}$ and $P_{\mathrm{sw,T34,tot}}$ are the total switching losses of T_1 and T_2, D_1 and D_2, and T_3 and T_4 (including the FWDs of T_3 and T_4), respectively.

In inverter mode of operation, Fig. 12(b), configuration A1 shows lower total conduction losses than configurations B1 and C1, however, due to considerably higher switching losses, the lowest operating switching frequency results for configuration A1. The losses calculated for the configurations A2, B2, and C2 are identical to the losses calculated for the configurations A1, B1, and C1 because in inverter mode of operation with unity power factor neither conduction losses nor switching losses change if SiC SBDs are used instead of Si diodes for D_1 and D_2. However, configurations B3 and C3 allow for higher switching frequencies due to the reduced total switching losses. For inverter mode of operation, configuration C3 allows for the highest switching frequency of 19.7 kHz. This is considerably less than the highest switching frequency feasible for rectifier mode of operation (32.5 kHz), which is due to the switching losses $E_{\mathrm{off,T12}}$, generated by the IGBTs T_1 and T_2.

V. Conclusion

In this paper, the total semiconductor losses of three-level T-type rectifier and inverter of a 20 kVA UPS system, are determined for different realizations of the bi-directional switches, i.e. with and without RB-IGBTs. In addition, the improvements feasible with SiC SBDs being used instead of Si diodes are analyzed and evaluated for 3LTTC topologies.

Comparison results show that the rectifier preferably employs RB-IGBTs for the bi-directional switch (low conduction losses) and SiC SBDs for the rectifier diodes (low switching losses). With this, switching frequencies up to 32.5 kHz are feasible for total semiconductor losses of the rectifier of 250 W. In inverter mode of operation with unity power factor, the converter configuration with the bi-directional switch being realized with an anti-series connection of standard IGBT / SiC SBD modules shows lowest total losses for switching frequencies greater than 8 kHz and is, therefore, considered most suitable. Still, further improvements of the RB-IGBT, in particular with respect to reverse recovery effects in order to reduce switching losses, e.g. by applying the latest generation's internal structure with life time control techniques, would change the results obtained in this comparison and may render the RB-IGBT better suitable for inverters based on the 3LTTC topology, too.

References

[1] J. Samstad and M. Hoff, "Technical comparison of on-line vs. lline-interactive ups designs," tech. rep., American Power Conversion, 2004.

[2] A. Nabae, I. Takahashi, and H. Akagi, "A new neutral-point-clamped pwm inverter," *IEEE Trans. on Ind. Appl.*, vol. 1A-17, pp. 518 – 523, September/October 1981.

[3] M. Schweizer, I. Lizama, T. Friedli, and J. W. Kolar, "Comparison of the chip area usage of 2-level and 3-level voltage source converter topologies," in *Proc. of the 36th Annu. Conf. of the IEEE Ind. Elec. Society (IECON 2010)*, (Phoenix, USA), November 2010.

[4] R. Maheshwari, S. Munk-Nielsen, and S. Busquets-Monge, "Emi performance comparison of two-level and three-level inverters in small dc-link capacitors based motor drives," in *IEEE Int. Symp. on Ind. Elec. (ISIE)*, 2012.

[5] T. Soeiro and J. W. Kolar, "Novel 3-level hybrid neutral-point-clamped converter," in *Proc. of the 37th Annu. Conf. of the IEEE Ind. Elec. Society (IECON 2011)*, (Melbourne, Australia,), November 2011.

[6] M. Takei, Y. Harada, and K. Ueno, "600v-igbt with reverse blocking capability," in *Proc. of 2001 Int. Symp. on Power Semiconductor Devices and ICs*, (Osaka, Japan), pp. 413–416, 2001.

[7] A. Lindemann, "A new igbt with reverse blocking capability," in *Rec. of the 9th European Conf. on Power Elec. and Appl. (EPE)*, pp. 27 – 29, Aug. 2001.

[8] M. Otsuki and Y. Seki, "The authentic reverse blocking igbt (rb-igbt) technologies for bi-directional switching applications," in *PCIM Brasil Conference*, 2012.

[9] M. Qingyun, M. Weiming, S. Chi, J. Guisheng, and Q. Wei, "Analytical calculation of the average and rms currents in three-level npc inverter with spwm," in *Proc. IEEE 35th Annu. Conf. Ind. Electron. Soc.*, pp. 243 – 248, 2009.

[10] J. Pou, J. Zaragoza, S. Ceballos, M. Saeedifard, and D. Boroyevich, "A carrier-based pwm strategy with zerosequence voltage injection for a three-level neutral-point-clamped converter," *IEEE Trans. on Power Elec.*, vol. 27, pp. 642 – 651, February 2012.

[11] F. Blaabjerg, J. K. Pedersen, S. Sigurjonsson, and A. Elkjaer, "An extended model of power losses in hard-switched igbt-inverters," in *Conf. Rec. 31st IEEE IAS Annu. Meeting*, vol. 3, pp. 1454 – 1463, October 1996.

[12] F. Schafmeister, C. Rytz, and J. W. Kolar, "Analytical calculation of the conduction and switching losses of the conventional matrix converter and the (very) sparse matrix converter," in *Proc. of the 20th Annu. IEEE Applied Power Elec. Conf. and Expo.*, vol. 2, pp. 875 – 881, March 2005.

[13] J. Lutz, H. Schlangenotto, U. Scheuermann, and R. D. Doncker, *Semiconductor Power Devices*. Springer, 2011.